"An aptamer-gated silica mesoporous material for thrombin detection" Oroval, M., Climent, E., Coll, C., Eritja, R., Aviñó, A., Marcos, M.D., Sancenón, F., Martínez-Máñez, R., Amorós, P. Chem. Comm., 49(48), 5480-5482 (2013).
PMID: 23660687; doi: 10.1039/C3CC42157K

An aptamer-gated silica mesoporous material for thrombin detection

Mar Oroval,[a,b,c] Estela Climent,[a,b,c] Carmen Coll,[a,b,c] Ramón Eritja,[c, d] Anna Aviñó,[c, d] Maria Dolores Marcos,[a,b,c] Félix Sancenón,[a,b,c] Ramón Martínez-Máñez,[a,b, c] Pedro Amorós[e]

[a]*Centro de Reconocimiento Molecular y Desarrollo Tecnológico (IDM), Unidad Mixta Universidad Politécnica de Valencia - Universidad de Valencia, Spain.*
[b]*Departamento de Química, Universidad Politécnica de Valencia, Camino de Vera s/n, 46022, Valencia, Spain. E-mail: rmaez@qim.upv.es*
[c]*CIBER de Bioingeniería, Biomateriales y Nanomedicina (CIBER-BBN)*
[d]*Institute for Research in Biomedicine (IRB Barcelona), CSIC, BaldiriReixac 10, E-08028 Barcelona, Spain.*
[e]*Institut de CiènciadelsMaterials (ICMUV), Universitat de Valencia, P.O. Box2085, E-46071 Valencia, Spain*

An aptamer-capped mesoporous material for the selective and sensitive detection of thrombin in human plasma and serum has been prepared and characterized.

The design of stimuli-responsive nanoscopic gated systems involving biomolecules has recently attracted great attention. In particular some biomolecules, especially enzymes,[i] have been used as stimuli to uncap gated-scaffolds whereas others such as saccharides,[ii] antibodies,[iii] peptides[iv] or DNA,[v] have been reported to act as capping agents. Capped materials have been mainly used in drug delivery applications. However examples of their use in sensing are by far much less common.[vi] In the latter approach the carrier system is loaded with a dye and the capped mechanism is designed in a way that only a target analyte is able to trigger the delivery of the cargo. Among different biomolecules that could act as caps aptamers are especially attractive for the design of gated nanosensors for sensing applications.[vii]

On the other hand thrombin is a coagulation protein that has many effects in the coagulation cascade and their determination can be used to understand thrombosis and hemostasis processes. This protein, also known as coagulation factor II, is a serine protease that converts soluble fibrinogen (factor I) into insoluble strands of fibrin (factor Ia).[viii, ix] The concentration of thrombin in blood varies considerably and can be almost absent in healthy subjects. However, during coagulation process, the concentration of thrombin in blood ranges from nM to low μM levels.[x] Moreover it is important to detect thrombin in blood serum for clinical and diagnostic applications.[xi]

Recently, various aptasensors based on electrochemistry,[xii] colorimetry,[xiii] fluorescence,[xiv] electrochemiluminescence,[xv] and other techniques[xvi] for thrombin detection have been developed. For instance, electrochemical aptasensors for thrombin detection based on nanoparticle labeling have been also described. For labeling purposes gold nanoparticles,[xvii] quantum dots[xviii] or carbon nanotubes[xix] have been widely used. One of the most commonly used aptamers, in the development of thrombin aptasensors, is the 15-mer DNA aptamer d(5-GGTTGGTGTGGTTGG-3), also known as thrombin-binding aptamer (TBA),[xx] which is able to bind selectively onto exosite I thrombin (fibrinogen binding sites) with highly specificity versus other substances.[xxi]

Despite the examples cited above, as far as we know, the use of TBA gated-hybrid mesoporous materials for the recognition of thrombin has not yet been reported. Taking these facts into account, in this work we present a new hybrid gated material for the fluorometric detection of thrombin. Based in our experience in the fields of bio-gated hybrid materials for sensing applications[xxii] we report herein the preparation of an aptamer-gated silica mesoporous supports for the selective and sensitive fluorogenic signalling of thrombin.

Scheme 1 shows the proposed paradigm for thrombin detection using capped mesoporous materials. MCM-41 mesoporous nanoparticles (diameter of ca. 100 nm) were selected as inorganic scaffold and the pores were loaded with a fluorophore (rhodamine B). Then the external surface of the loaded support was functionalized with 3-aminopropyltriethoxysilane (APTS) (solid **S1**). Aminopropyl moieties are partially charged at neutral pH and should display electrostatic interactions with the negatively charged TBA aptamer. Addition of TBA yielded the final capped hybrid material **S1-TBA**. In particular for the preparation of the gated material **S1-TBA**, 1.5 mg of **S1** were suspended in 1.5 mL of simulated human blood plasma (pH 7.25).[xxiii] Then, 60 µl of TBA (28 µM) were added to 150 µl of the **S1** suspension. The final **S1-TBA** solid was isolated by centrifugation and washed with 300 µl of simulated human blood plasma to eliminate the residual dye and the free TBA.

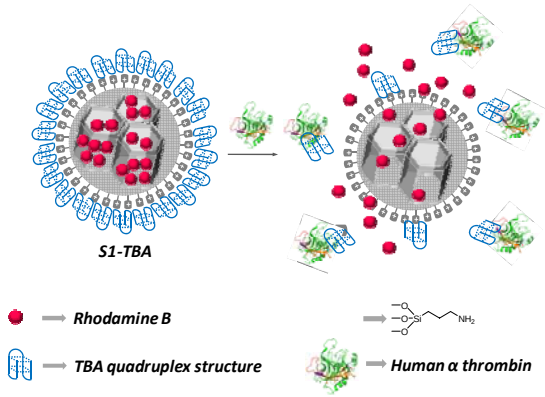

Scheme 1. Schematic representation of the gated material **S1** functionalised with 3-aminopropiltriethoxysilane and capped with TBA aptamer in quadruplex state (**S1-TBA**). The delivery of the entrapped guest (rhodamine B) is observed in the presence of thrombin.

S1 was characterized using standard procedures. X-ray pattern of **S1** shows the mesoporous characteristic (100) peak diffraction indicating that the loading process with the dye and the further functionalization with APTS have not damaged the mesoporous scaffolding (see Figure S2). The presence in the final functionalized solids of the mesoporous structure is also clearly observed from the TEM analysis (see Figure S2). The N_2 adsorption-desorption isotherms of the calcined MCM-41 nanoparticles (Figure S3) showed an adsorption step at an intermediate P/P_0 value (0.1 – 0.3). From this curve a pore volume of 0.84 $cm^3\ g^{-1}$ was calculated by using the BJH model on the adsorption branch of the isotherm. The application of the BET model resulted in a value for the total specific surface area of 1066.8 $m^2\ g^{-1}$. From the XRD, porosimetry and TEM measurements a pore diameter of 2.57 nm was determined. The N_2 adsorption-desorption isotherm of **S1** is typical of mesoporous systems with filled mesopores (see Figure S3), and a significant decrease in the N_2 volume adsorbed and a surface area (77 $m^2\ g^{-1}$) was observed.

The content of dye and APTS on solid **S1** were determined by elemental analysis and thermogravimetric studies and amounts to 0.092 and 1.65 mmol/g solid, respectively. Additionally, the content of TBA in solid **S1-TBA** was determined through the use of aptamer TBA-flu (5-GGTTGGTGTGGTTGG-fluorescein-3), similar to TBA but functionalized with a fluorescein dye. By following the decrease in absorbance of TBA-flu in the solution after the capping process and monitoring the TBA-flu released during uncapping experiments (see SI for details), we were able to calculate a TBA content of 0.016 mmol/g solid.

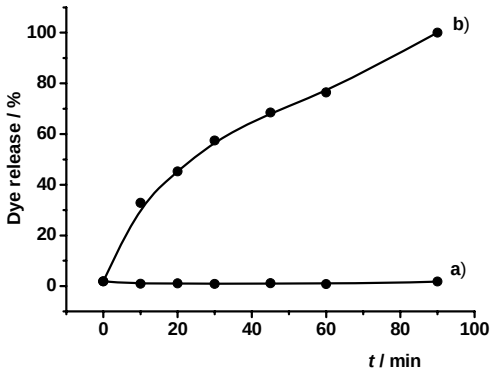

Figure 1. Release profile of rhodamine B from solid **S1-TBA** in absence (a) and in presence (b) of thrombin (2.89 μM) in simulated human blood plasma (pH 7.25).

In order to investigate the gating properties of **S1-TBA**, 150 μg of **S1-TBA** were suspended in 1.5 mL of simulated human blood plasma and the suspension was divided into two fractions. The first fraction was diluted with 286 μL of Milli-Q water, the second one was treated with 286 μL of an aqueous solution containing 2.89 μM of thrombin. In both cases the suspensions were stirred for 90 minutes at 37°C and a certain time intervals fractions were taken and centrifuged to remove the solid. Dye delivery at a certain time was then measured via the fluorescence emission of the rhodamine in the solution at 572 nm (λ_{exc} 555 nm). The delivery kinetics profile of rhodamine B in the presence and absence of the target protein thrombin is displayed in Figure 1. In absence of thrombin (curve a) solid **S1-TBA** shows a negligible dye release, indicating tight pore closure. On the other hand, the delivery of the dye is induced when thrombin is present in the solution due to displacement of the aptamer from the nanoparticles as consequence of aptamer-thrombin recognition (curve b). At 60 minutes ca. 80% of the delivery was reached (31% of the total adsorbed rhodamine B in solid **S1-TBA**).

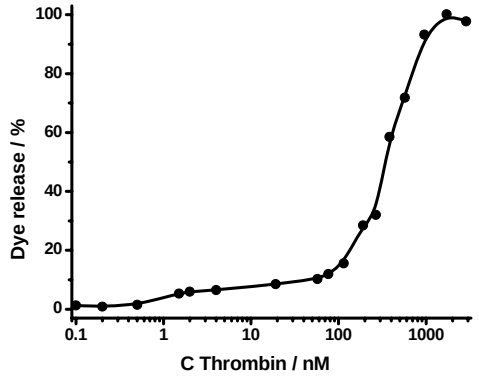

Figure 2. Release of rhodamine B from **S1-TBA** as a function of the concentration of thrombin added (after 60 min of reaction) in simulated human blood plasma (pH 7.25).

Following a similar procedure delivery of rhodamine B from **S1-TBA** as a function of the amount of thrombin and the results are shown in Figure 3. As it can be seen the cargo delivered is proportional to thrombin concentration in agreement with the uncapping protocol detailed above. The maximum delivery was observed at a concentration of 1700 nM of thrombin. Finally, a limit of detection of 2 nM (3σ) of thrombin was found.

The use of gated materials for sensing applications has as an specialfeature to separates the recognition protocol (in our case the formation of TBA-protein pair) from the signalling event making sensing independent of the stocichiometry of the host-guest complex and sometimes displaying features of signal enhancement. In our particular case, at low thrombin concentrations (ca. 4 nM), one molecule of thrombin was able to deliver ca. 115 molecules of dye, which is a remarkable sign of signal amplification.

The *in vitro* characterization of the nanodevice suggested that **S1-TBA** nanomaterial is sensitive to the presence of thrombin. Moreover, in order to study the possible application in the detection of thrombin in biological samples, **S1-TBA** was tested using commercially available human serum (from human male AB plasma). In a first step, the tolerance of the solid to human serum was studied, suspending 1 mg of **S1-TBA** in 1 mL of serum diluted with PBS (40, 20, 10 and 5%). From these measurements a 10% serum dilution showed the best response with a limit of detection as low as 4 nM of thrombin (3σ; see Figure S4 and experimental details in the SI). In a second step, with the aim to verify the feasibility of the developed method, we prospectively used solid **S1-TBA** for the determination of thrombin in human serum. For this purpose, in a typical experiment, human serum samples were spiked with 75, 150 and 300 nM of thrombin,

respectively. Samples were diluted with PBS for a final amount of 10%, and the contents of human thrombin were determined with **S1-TBA** material using the addition standard method. The obtained results are shown in Table S1. Remarkable recoveries in the range of 91-120% of thrombin were achieved.

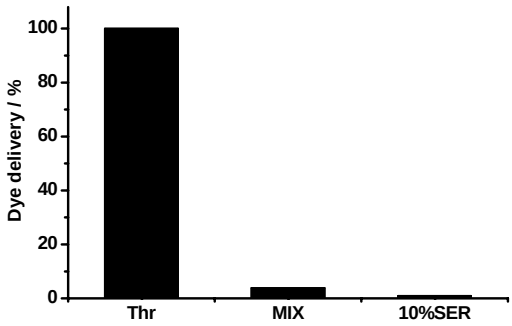

Figure 3. Fluorescence of rhodamine B released from **S1-TBA** suspensions (in PBS containing 10% human serum) in the presence of thrombin (56 nM), and a mixture of OVA and BSA (56 nM) after 15 minutes of the addition. For comparative purposes the release of rhodamine B from S1-TBA suspensions in PBS containing 10% human serum is also shown.

In order to further investigate the selectivity of **S1-TBA** material control release experiments in the presence of other non-specific binding proteins (OVA and BSA) were carried out. In particular, PBS containing 10% of human serum was spiked with 56 nM of OVA and BSA and the rhodamine B released after 15 min measured. Figure 3 showed that a mixture of OVA and BSA was unable to induce the uncapping of the pores, observation that reinforces the selective thrombin-TBA interaction as the mechanism of the fluorogenic response observed.

In conclusion, we have prepared an aptamer-gated delivery system (**S1-TBA**) for the fluorogenic detection of thrombin. The sensing mechanism arises from the high affinity between an aptamer (TBA) and its target protein (thrombin). In vitro studies with **S1-TBA** showed a limit of detection of 2 nM (3σ) for thrombin. In addition the hybrid nanomaterial allowed accurate thrombin detection in human serum diluted with PBS also with high sensitivity (limit of detection of 4 nM (3σ)). The method, based in a simple competitive procedure is undemanding and suggested that the use of aptaners could be a suitable approach to develop gated nanoparticles for simple chromo-fluorogenic assays for a wide range of bio-applications.

The authors thank the Spanish Government (project MAT2012-38429-C04-01) the Generalitat Valenciana (project PROMETEO/2009/016) and the CIBER-BBN for their support.

Supporting Information

An aptamer-gated silica mesoporous material for thrombin detection

Mar Oroval, Estela Climent, Carmen Coll, Ramón Eritja, Anna Aviñó, Maria Dolores Marcos, Félix Sancenón, Ramón Martínez-Máñez, Pedro Amorós.

Chemicals

The chemicals tetraethylorthosilicate (TEOS), n-cetyltrimethylammonium bromide (CTABr), sodium hydroxide (NaOH), rhodamine B, 3-aminopropiltriethoxysilane and human serum – from human male AB plasma (sterile-filtered) were provided by Aldrich. The aptamers TBA d(5- GGTTGGTGTGGTTGG -3) and **TBA-flu** d(5-GGTTGGTGTGGTTGG-fluorescein-3) were provided by the group of Nucleic Acids from the Institute for Research in Biomedicine of Barcelona (IRB Barcelona). Analytical-grade solvents were from Scharlab (Barcelona, Spain). All reactives were used as received.

General Techniques

XRD, TG analysis, elemental analysis, TEM microscopy, N_2 adsorption-desorption and UV-visible spectroscopy techniques were employed to characterize the prepared materials. X-ray measurements were performed on a Brücher AXS D8 Advance diffractometer using Cu-Kα radiation. Thermo-gravimetric analysis were carried out on a TGA/SDTA 851e Mettler Toledo equipment, using an oxidant atmosphere (Air, 80 mL/min) with a heating program consisting on a heating ramp of 10 °C per minute from 393 K to 1273 K and an isothermal heating step at this temperature during 30 minutes. TEM images were taken with a JEOL TEM-1010 Electron microscope working at 100 kV. N_2 adsorption-desorption isotherms were recorded on a Micromeritics ASAP2010 automated sorption analyser. The samples were degassed at 120ºC in vacuum overnight. The specific surfaces areas were calculated from the adsorption data in the low

pressures range using the BET model. Pore size was determined following the BJH method. UV-visible spectroscopy was carried out with a Jasco V-630 Spectrometer. Fluorescence spectroscopy was carried out on a Jasco FP-8300 Spectrometer and UV-visible spectroscopy was carried out with a Jasco V-630 Spectrometer.

Buffer Solutions

Phosphate buffered saline 1x (PBS 1x) consisting in 137 mM NaCl, 1.47 mM KH_2PO_4, 7.85 mM Na_2HPO_4, 2.68 mM KCl (pH:7.5) was used for controlled release experiences.

Synthesis of the silica mesoporous nanoparticles support (SMPS)

The MCM-41 mesoporous nanoparticles were synthesized by the following procedure: n-cetyltrimethylammoniumbromide (CTABr, 1.00 g, 2.74 mmol) was first dissolved in 480 mL of deionized water. Then a 3.5 mL of NaOH 2.00 M in deionized water was added to the CTABr solution, followed by adjusting the solution temperature to 80ºC. TEOS (5 mL, 2.57. 10-2 mol) was then added dropwise to the surfactant solution. The mixture was allowed stirred for 2 h to give a white precipitate. Finally the solid product was centrifuged, washed with deionized water and was dried at 60ºC (MCM-41 as-synthesized). To prepare the final porous material (MCM-41), the as-synthesized solid was calcined at 550 ºC using oxidant atmosphere for 5 h in order to remove the template phase.

Synthesis of S1

The amino-functionalised solid **S1** was prepared following literature procedures. 500 mg of calcined MCM-41 and 33.2 mg (0.10 mmol) of dye rhodamine B were suspended in 40 mL of acetonitrile inside a round-bottom flask connected to a Dean-Stark in an inert atmosphere. The suspension was refluxed (110 ºC) in azeotropic distillation, collecting 10 mL in the trap in order to remove the adsorbed water. Then, the mixture was stirred during 24 hours at 36ºC with the aim of achieving maximum loading in the pores of the MCM-41 scaffolding. Afterward an excess of 3-aminopropiltriethoxysilane (APTS, 0.936 mL, 4.0 mmol) was added, and the suspension was stirred for 5.5 h. Finally, the pink solid (**S1**) was filtered off and dried at 70 ºC for 12h.

Synthesis and optimization of solid S1-TBA

In order to estimate the proper amount of TBA for the preparation of **S1-TBA**, capping and release experiments in presence of different amounts of TBA were carried out. First of all, portions of 50 μL of a suspension of 1 mg **S1**/1 mL PBS were added to a solution containing the aptamer **TBA-flu** d(5- GGTTGGTGTGGTTGG -fluorescein-3) in concentrations of (0.02, 0.04, 0.06 and 0.08 μmol of **TBA-flu** g solid^{-1}) in Milli-Q water, and each suspension was stirred during 30 min at 37ºC, respectively. Afterwards, the absorbance of **TBA-flu** in the solution after the capping process was measured, in order to estimate the content of **TBA-flu** retained into solid. Results are shown in Table S1.

Table S1. Content of TBA added for the synthesis of **S1-TBA** and TBA retained during the process in mmol g^{-1} S1.

TBA added (mmol g^{-1} S1)	**TBA retained (mmol g^{-1} S1)**	**% retained (mmol g^{-1} S1)**
0.02	0.0123	61.55
0.04	0.0164	44.25
0.06	0.0134	22.44
0.08	0.0027	3.43

For study the release properties of the prepared solids, some release studies were carried. The isolated solids were divided in two parts. To one part, a solution of 250 μL PBS 1x containing human α thrombin in concentrations of: 0.04, 0.06 and 0.08 μmol of thrombin g solid^{-1}; to the other part 250 μL PBS 1x were added. The suspensions were stirred for one hour; during this period two aliquots of the suspensions were taken. Finally, after centrifugation of all the aliquots the fluorescence of rhodamine B emission at 572 nm (λex = 555nm) delivered to the solution was measured. It was found that all the concentrations were able to induce an effective capping of the pores, but in terms of dye release the concentration of the TBA at 0.04 mmol g^{-1} S1, showed more dye delivery than the others two TBA concentrations (0.06 and 0.08 mmol g^{-1} S1). Results are collected in Figure S1.

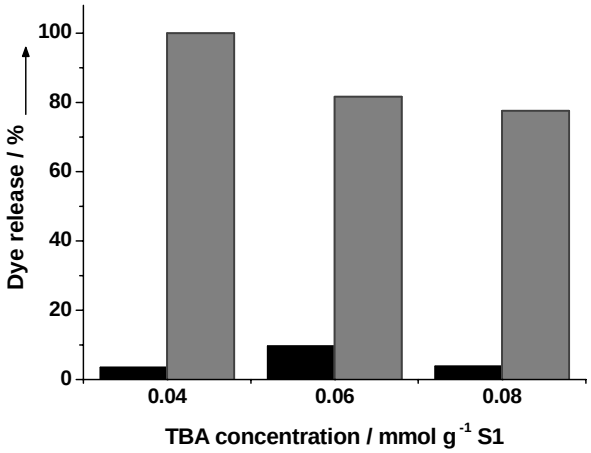

Figure S1. Optimization of the concentration of TBA to reach an effective capping of the pores. The black bars represent the blanks (absence of thrombin) and the grey bars represent the samples in presence of thrombin 0.04, 0.06 and 0.08 μmol of thrombin g solid^{-1}, respectively. All the measurements were carried out in PBS 1x (pH 7.5).

With the aim to obtain solid **S1-TBA**, 50 μL of a suspension of 1 mg **S1** in 1 mL PBS were suspended in 20 μl of a solution containing the aptamer TBA d(5-GGTTGGTGTGGTTGG -3) in a concentration of 28.57 μM in Milli-Q water, and the suspension was stirred at 37ºC during 30 min. The final **S1-TBA** solid was isolated by centrifugation and washed with 100 μL of PBS buffer (pH 7.5) in order to remove the residual dye and the free aptamer TBA.

Materials Characterization

Solid **S1** was characterized using standard procedures. Figure S2 shows powder X-ray patterns of the nanoparticulated MCM-41 as made support, calcined MCM-41 and the **S1** functionalized material. The PXRD of siliceous nanoparticulated MCM-41 as-synthesized (curve a) shows four low-angle reflections typical of a hexagonal array that can be indexed as (100), (110), (200), and (210) Bragg peaks. A significant displacement of the (100) peak in the XRD powder of the nanoparticulated MCM-41 calcined sample is clearly appreciated in the curve b, corresponding to an approximate cell contraction of 6.6 Å. This displacement and the broadening of the (110) and (200) peaks are related to further condensation of silanol groups during the calcination step. Finally, curve c corresponds to the **S1** XRD pattern. In this case, a little loss of the (110) and (200) reflections is observed, most likely related to a loss of contrast due to the

filling of the pore voids with the rhodamine B dye. Nevertheless, the value and intensity of the (100) peak in this pattern strongly evidences that the loading process with the dye and the further functionalization with APTS have not damaged the mesoporous 3D MCM-41 scaffolding.

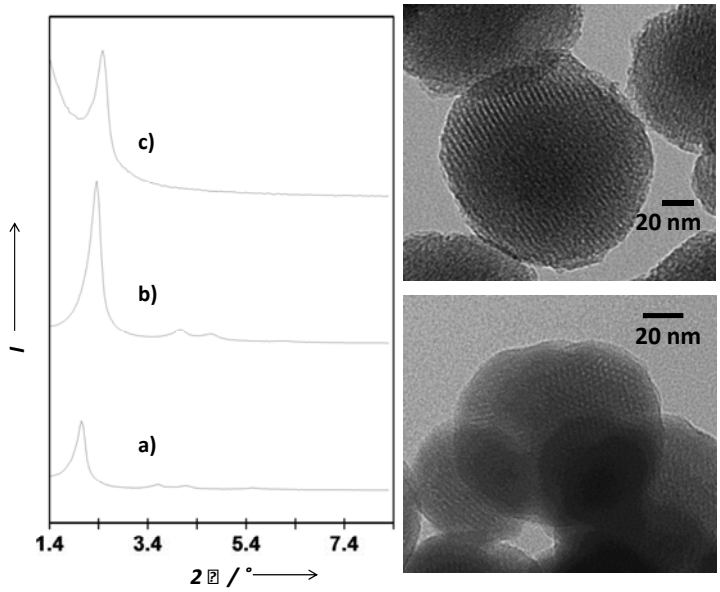

The presence in the final functionalized solids of the mesoporous structure is also confirmed from the TEM analysis, in which the typical channels of the MCM-41 matrix are visualized as alternate black and white stripes (see Figure S2 for MCM-41 calcined and solid **S1**). The figure also shows that the prepared MCM-41 and solid **S1** are obtained as spherical particles with diameters ranging from 100 to 200 nm.

Figure S2. Left: powder X-ray patterns of the solids (a) MCM-41 as synthesized (b) calcined MCM-41 and (c) solid **S1** containing the dye rhodamine B and 3-aminopropiltriethoxysilane. Right: TEM images of (a) calcined MCM-41 sample and (b) solid **S1** showing the typical hexagonal porosity of the MCM-41 mesoporous matrix.

The N_2 adsorption-desorption isotherms of the nanoparticulated MCM-41 calcined material shows two sharp adsorption steps. The isotherm shows a first step at intermediate P/P_0 value (0.1-0.3) typical of these solids (see Figure S3, curve a). This step can be related to the nitrogen condensation inside the mesopores by capillarity. The absence of a hysteresis loop in this interval and the narrow BJH pore distribution suggests the existence of uniform cylindrical mesopores with pore volume of 0.84 cm^3 g^{-1} calculated by using the BJH model on the adsorption branch of the isotherm. The application of the BET model resulted in a value for the total specific surface of 1066.8 m^2 g^{-1}. From the XRD, porosimetry and TEM studies, the a_0 cell parameter (43.16 Å), the pore diameter (2.57 nm) and a value for the wall thickness (1.74 nm) were calculated. In addition to this adsorption step associated to the micelle generated mesopores, a second feature appears in the isotherm at a high relative pressure ($P/P_0 >$ 0.8). This adsorption correspond to the filling of the large voids among the particles and present a volume of 0.47 cm^3 g^{-1} (calculated by using the BJH model) and then must be considered as a textural-like porosity. In this case, the curves show a characteristic H1 hysteresis loop and a wide pore size distribution.

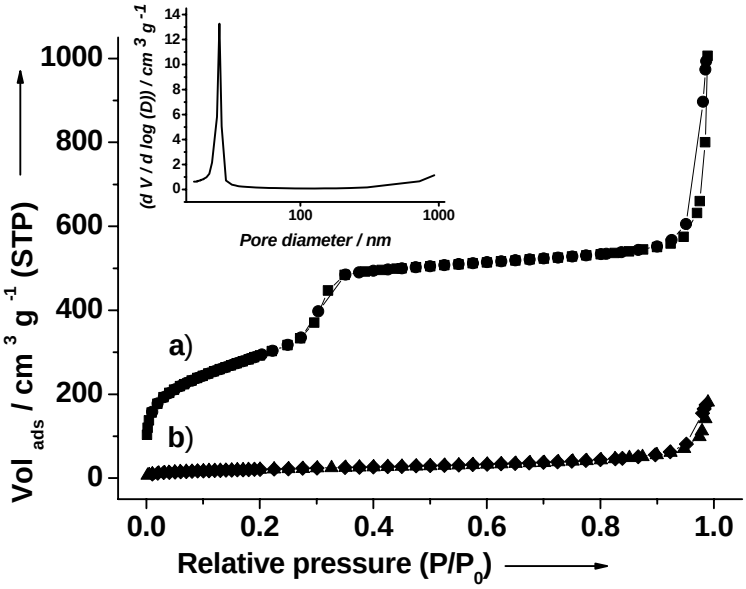

Figure S3. Nitrogen adsorption-desorption isotherms for (a) MCM-41 mesoporous material and (b) **S1** material. Inset: Pore size distribution of MCM-41 mesoporous material.

The N_2 adsorption-desorption isotherm of **S1** is typical of mesoporous systems with filled mesopores (see Figure 7, curve b), and a significant decrease in the N_2 volume adsorbed and surface area (0.06 cm^3 g^{-1} and 77.1 m^2 g^{-1} respectively) is observed. The most relevant feature is the absence of a sharp step at low-medium relative pressure ($0.1 < P/P_0 < 0.4$). In fact, this solid shows flat curves when compared (at the same scale) to those of the MCM-41 parent material, this indicates a significant pore blocking and the subsequent absence of appreciable mesoporosity. Additionally, a certain textural porosity is preserved. BET specific surface values, pore volumes, and pore sizes calculated from the N_2 adsorption-desorption isotherms for MCM-41 and **S1** are listed in Table S2.

Table S2. BET specific surface values, pore volumes and pore sizes calculated from the N_2 adsorption-desorption isotherms for selected materials.

	S_{BET} (m^2 g^{-1})	**Pore Volume** [a] (cm^3 g^{-1})	**Pore size** [a] (nm)

MCM-41	1066.8	0.84	2.57
S1	77.1	0.06	-

[a] Volume (V) and diameter (D) of mesopore.

The content of APTS and rhodamine B in the prepared solids **S1** and **S1-TBA**were determined by elemental analysis, thermogravimetric and delivery studies. The content of dye in solid **S1-TBA**was determined from the rhodamine B released during the capping process of **S1** with TBA, by measuring the absorbance of the released dye during the washing process. Values of content are detailed in Table S3. The thermal analysis of the **S1** shows typical behaviour in functionalised mesoporous materials; i.e. a first weight loss between 25 and 150ºC related to the solvent evolution, a second step, between 150 and 800 ºC due to the combustion of the organics and a final loss in the 800 - 1000 ºC range related to the condensation of the silanol groups. In addition, from elemental analysis of C, H, N, S it is possible to determine the amount 3-aminopropyltriethoxysilane and rhodamine B contained in the materials calculated in millimole per gram of S1 (mmol g^{-1} S1) using equation 1:

$$\alpha_A = \frac{\Delta M_i\% \; x \; 1000}{n M_i} \qquad \left(\frac{mmol}{g\ S1}\right) \qquad (1)$$

where $\Delta Wi\%$ (i = C, N, S) are the weight percentages of carbon, nitrogen or sulphur, M_i is the corresponding atomic weight and n is the number of the corresponding atom type in one molecule. In addition, the content of dye in solid **S1-TBA** was determined from the dye content in **S1** after interaction with TBA aptamer, and determining the amount of dye delivered when washing the solids. Also, the amount of dye delivered from **S1-TBA** in the presence of thrombin was determined by using values of intensity of the fluorescence bearing in mind that, at low concentrations, relation between concentration and intensity are linear. Values of content are detailed in Table S3.

Table S3. Content of APTS and rhodamine B in the prepared solids **S1** and **S1-TBA**in mmol/g SiO_2.

Solid	α_{APTS} (mmol / g S1)	$\alpha_{Rhodamine\ B}$ (mmol / g S1)	α_{TBA} (mmol / g S1)
S1	1.65	0.092	-
S1-TBA	1.65	0.057	0.0164

Taking into account the different amounts of APTS and aptamer TBA in solid **S1-TBA** it is possible to estimate the distribution of aptamer onto surface. Using these values, we can estimate that **S1-TBA** material contains 9.87 x 10^{18} oligonucleotide molecules/g solid. Additionally, considering surface value of **S1** calculated from N_2 adsorption measurements (77.1 m^2/g) and the aptamer content calculated previously, the average surface coverage on solid **S1-TBA** by aptamer molecules is 0.36 molecules/nm^2. This aptamer surface coverage resulted in an average distance between aptamer molecules of about 2.8 nm. On the other hand, and bearing in mind again a typical value of external surface of **S1** (77.1 m^2/g) and the content of APTS (in mmol/g SiO_2) calculated with elemental analysis and thermogravimetric studies, the average surface coverage on solid **S1-TBA** by APTS molecules is 12.8 molecules/nm^2. Finally, using the aptamer and APTS contents calculated previously a ratio of 100 APTS molecules/aptamer molecule was estimated.

In vitro characterization of S1-TBA in human serum

The delivery experiments of **S1-TBA** in human blood plasma showed faster response than the response observed in simulated human blood plasma (related with stronger ionic strength), showing a tolerance of the system using 10% of human serum. Calibration curve for thrombin containing 10 % of human serum was obtained(Figure S4), showing the maximum delivery of the dye at 15 min employing 98.82 nM of thrombin.

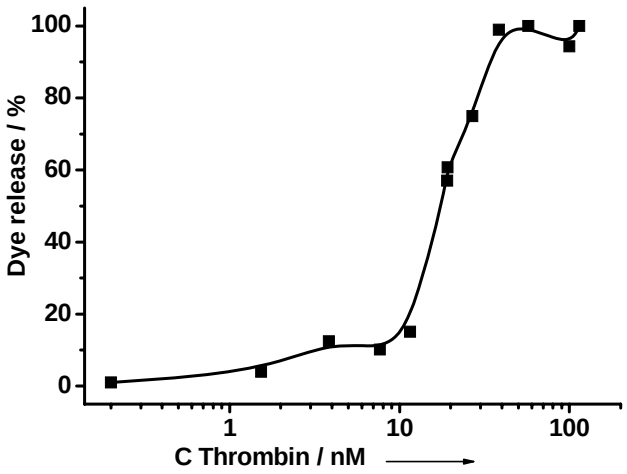

Figure S4. Release of rhodamine B from solid **S1-TBA** in function of the concentration of human α thrombin in PBS containing 10% of human serum – from human male AB plasma.

Determination of thrombin in human serum

Table 1. Determination of thrombin in 10% human serum samples.

Thrombin added (nM)	Thrombin found (nM)	Recovery
75	68.35 ± 5.56	91
150	147.32 ± 4.08	98
300	361.22 ± 60.47	120

[i] a) K. Patel, S. Angelos, W. R. Dichtel, A. Coskun, Y. –W. Yang, J. I. Zink, J. F. Stoddart, *J. Am. Chem. Soc.,* **2008***, 130*, 2382. b) A. Schlossbauer, J. Kecht, T. Bein, *Angew. Chem. Int. Ed.*, **2009**, *48*, 3092. c) A. Bernardos, E. Aznar, M. D. Marcos, R. Martínez-Máñez, F. Sancenón, J. Soto, J. M. Barat, P. Amorós, P. *Angew. Chem. Int. Ed.*, **2009**, *48*, 5884. d) C. Park, H. Kim, S. Kim, C. Kim, *J. Am. Chem. Soc.,* **2009**, *131*, 16614. e) P. D. Thornton, A. Heise, *J. Am. Chem. Soc.,* **2010**, *132*, 2024.

[ii] A. Bernardos, L. Mondragón, E. Aznar, M. D. Marcos, R. Martínez-Máñez, F. Sancenón, J. Soto, J. M. Barat, E. Pérez-Payá, C. Guillem, P. Amorós, *ACS Nano*, **2010**, *4*, 6353.

[iii] a) E. Climent, A. Bernardos, R. Martínez-Máñez, A. Maquieira, M. D. Marcos, N. Pastor-Navarro, R. Puchades, F. Sancenón, J. Soto, P. Amorós, *J. Am. Chem. Soc.* **2009**, *131*, 14075. b) E. Climent, R. Martínez-Máñez, A. Maquieira, F. Sancenón, M. D. Marcos, E. M. Brun, J. Soto, P. Amorós, *Chem. Open* **2012**, 1, 251. c) E. Climent, D. Gröninger, M. Hecht, M. A. Walter, R. Martínez-Máñez, M. G. Weller, F. Sancenón, P. Amorós, and K. Rurack, *Chem. Eur. J.* **2013,** DOI: 10.1002/chem.201300031.

[iv] a) C. Coll, L. Mondragón, R. Martínez-Máñez, F. Sancenón, M. D. Marcos, J. Soto, P. Amorós, E. Pérez-Payá, *Angew. Chem. Int. Ed.*, **2011**, 50, 2138. b) F. Porta, G. E. M. Lamers, J. I. Zink, A. Kros, *Phys. Chem. Chem. Phys.,* **2011**, *13*, 9982.

[v] a) A. Schossbauer, S. Warncke, P. M. E. Gramlich, J. Kecht, A. Manetto, T. Carell, T. Bein, *Angew. Chem.Int. Ed.*, **2010**, *49*, 4734. b) Y. Zhang, Q. Yuan, T. Chen, X. Zhang, Y. Chen, W. Tan, *Anal. Chem.*, **2012**, *84*, 1956.

[vi] a) E. Climent, A. Bernardos, R. Martínez-Máñez, A. Maquieira, M. D. Marcos, N. Pastor-Navarro, R. Puchades, F. Sancenón, J. Soto, P. Amorós, *J. Am. Chem. Soc.* **2009**, *131*, 14075-14080. E. Climent, D. Gröninger, M. Hecht, M. A. Walter, R. Martínez-Máñez, M. G. Weller, F. Sancenón, P. Amorós, and K. Rurack, *Chem. Eur. J.* **2013,** DOI: 10.1002/chem.201300031.

[vii] a) C. -L. Zhu, C. –H. Lu, X. –Y. Song, H. –H. Yang, X. –R. Wang, *J. Am. Chem. Soc.*, **2011**, *133*, 1278. b) V. C. Özalp, T. Schäfer, *Chem. Eur. J.,* **2011**, *17*, 9893

viii C. A. Holland, A. T. Henry, H. C. Whinna, F.C. Church, *FEBS Lett.* **2000**,*484*, 87.

ix L. Francois, F.W. David, *Physiol. Rev.,* **1954**, *34*, 722.

x M.A. Shuman, P.W. Majerus, *J. Clin. Invest.* **1976**, *58*, 1249.

xi a) J. Zheng, G.-F. Chen, P.-G. He, Y.-Z.Fang, *Talanta*, **2010**, *80*,1868. b) Y. Wang, X.He, K. Wang, X. Ni, J. Su, Z. Chen, *Biosens. Bioelectron.* **2011**, *26*, 3536.

[xii] a) P.L. He, L. Shen, Y.H. Cao, D.F. Li, *Anal. Chem.* **2007**, *79*, 8024. b) J. Zhao, Y. Zhang, H. Li, Y. Wen, X. Fan, F. Lin, L. Tan, S. Yao, *Biosens. Bioelectron.* **2011**, *26*, 2297.

xiii a) C.-K. Chen, C.-C. Huang, H.-T. Chang, *Biosens. Bioelectron.*, **2010**, *25*, 1922. b) T. Li, E. Wang, S. Dong, *Chem. Commun.* **2008**, 3654.

xiv a) H.X. Chang, L.H. Tang, Y. Wang, J. H. Jiang, J.H. Li, *Anal.Chem.* **2010**, *82*, 2341. b) K. A. Edwards, Y. Wang, A. J. Baeumner, *Anal Bioanal. Chem,* **2010**, 398, 2645.
xv a) X.-B.Yin, Y.-Y.Xin, Y. Zhao, *Anal. Chem.*, **2009**, *81*, 9299. b) L. Fang, Z. Lü, H. Wei, E. Wang, *Anal. Chim. Acta,* **2008**, *628*, 80. c) J.Wang, Y-Y. Shan, W. Zhao, J-J. Xu, H-Y. Chen, *Anal. Chem.* **2011**, *83*, 4004.
xvi a) Q. Zhao, X.F. Lu, C.-G. Yuan, X.-F. Li, X.C. Le, *Anal.Chem*., **2009**, *81*, 7484. b) J. Hu, P.-C. Zheng, J.-H. Jiang, G.-L.Shen, R.-Q. Yu, G.-K. Liu, . *Anal. Chem.* **2009**, *81*, 87.
xvii C.F. Ding, Y. Ge, J. –M. Lin, *Biosens. Bioelectron.*, **2010**, *25*, 1290.
xviii a) C.F. Ding, Y. Ge, S.S. Zhang, *Chem. Eur. J.,* **2010**, *16*, 10707. b) Y. H. Tennico, D. Hutanu, M. T. Koesdjojo, C. M. Bartel, V. T. Remcho, *Anal. Chem.,* **2010**, *82*, 5591.
xix M.M. Teresa, Y.-C. Tseng, N. Ormategui, I. Loinaz, R. Eritja, J. Bokor, *Nano Lett.,* **2009**, *9*, 530.
xx L. C. Bock, L. C. Griffin, J. A. Latham, E. H. Vermaas, J. J. Toole, *Nature*, **1992**, *355*, 564.
xxi a)W. Bode, D. Turk, A. Karshikov, *Protein Sci.,* **1992**, *1*, 426. b) M.T. Stubbs, W. Bode, *Thromb. Res.,* **1993**, *69*, 1.
xxii E. Climent, R. Martínez-Máñez, F. Sancenón, M. D. Marcos, J. Soto, A. Maquieira, P. Amorós, *Angew. Chem. Int. Ed.* **2010**, *49*, 7281.
xxiii M. R. C. Marques, R. Loebenberg, M. Almukainzi, *Dissolution Technologies,* **2011**, *18*, 15.